Heliyon 10 (2024) e38963

Contents lists available at ScienceDirect

Heliyon

journal homepage: www.cell.com/heliyon

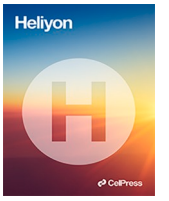

Research article

The investigation of an inspired type toroidal dipole flexible metasurfaces at terahertz frequencies

Shuang Wang [*], Hai Huang, Quan Li [**], Chen Wang, Han Lei [***]

School of Electronic Engineering, Tianjin University of Technology and Education, Tianjin, 300222, China

ARTICLE INFO

Keywords:
Toroidal dipole
Terahertz
Metasurfaces
The scattering power of the multipoles

ABSTRACT

We theoretically and experimentally carried out an inspired type of toroidal dipole (TD) metasurfaces, which composed of a metamolecule of symmetric aluminium semicircles with a bar in the middle fabricated on polyimide substrate in the terahertz (THz) regime. It was found that the three resonances show red-shift tendency due to the increase of inductance and capacitance with the increase of semicircle's outer radius. Meanwhile, both the TD resonances and the current flowing in the metallic bar can generate the head-to-tail magnetic field distribution, which is the most prominent feature of TD phenomenon. The generation of this phenomenon is discussed deeply via the power of the multipoles, which are calculated according to the volume current density distribution data extracted from the simulations. The low frequencies (~0.5 THz) head-to-tail magnetic field distribution is mainly attributed to TD resonance generated via the mutual effect between the two semicircles, while the same phenomenon at high frequencies (~0.8 THz) is mainly attributed to the current flowing the middle metallic bar. The enhancement of head-to-tail magnetic field distribution leads to the increase of quality (Q) factor, and the Q factor of fabricated sample is as high as 24.5. Moreover, the electromagnetic properties in TD metasurfaces could be adjusted by the metal bar's width. The optimization of TD resonances provides opportunity to design the high Q-factor metasurfaces, and it opens up potential applications in terahertz high sensitivity devices.

1. Introduction

Toroidal electromagnetic phenomenon has become a new branch of the electromagnetic research field, since Zel' Dovich come up with the theory of toroidal electromagnetic phenomenon in 1950's [1]. Compared with the higher order toroidal electromagnetic phenomenon, toroidal dipole (TD) is the simplest type in the toroidal families, which has attracted more attention since a few years ago [2–6]. TD are characterized by the flow of poloidal currents on a torus' meridians, and poloidal currents produce magnetic dipoles arranged in head-to-tail configurations. Significantly, TD has some unique characteristics, such as nonradiative resonance, high quality (Q) factor and so on, which has potential application in the electromagnetic functional devices [7–11]. However, the TD is often weak in the nature, and often masked by the other stronger electric/magnetic multipoles, that is why the toroidal moment family is the latest electromagnetic family detected by the researchers.

* Corresponding author.
** Corresponding author.
*** Corresponding author.
E-mail addresses: wangshuang@tute.edu.cn (S. Wang), quanli@tute.edu.cn (Q. Li), hanleigeneva@163.com (H. Lei).

https://doi.org/10.1016/j.heliyon.2024.e38963
Received 20 June 2024; Received in revised form 2 October 2024; Accepted 3 October 2024
Available online 4 October 2024

Table 1
The comparative analysis of previous TD metamaterials at terahertz frequencies.

Ref	Frequency (THz)	Simulation(S) /Fabrication (F)	Structure of unit cell	Flexible	Substrate	Q value	Virtues
40	1–1.6	S	Silicon structure	No	Quartz	>1100	QBIC
44	~200	F	Silicon structure	No	Glass/No	4990	QBIC
43	0.9–1	S	Slot rings	Yes	PDM	≥14	Ultra-high Q-factors
3	0.2–0.8	F	Aluminum metal patterns	No	Silicon	32	Asymmetric Fano structure
51	0.2–2	S	Two metallic patterns on each side of polyimide	Yes	Polyimide	38.1	Slow light plateaus
53	0.6–1.5	F	Two symmetric C-rings	Yes	Polyimide	22.5	Flexible Metasurfaces
20	0–1.2	F	Four asymmetric split-ring resonators	Yes	Polyimide	Not mentioned	The mutual effect between two metallic layers.

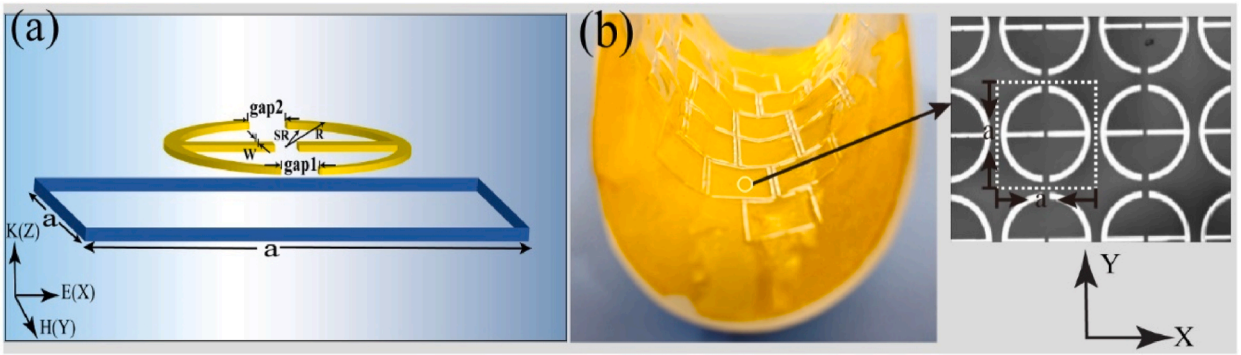

Fig. 1. (a) Schematic diagram of the high Q-factor TD metasurfaces unit structure, (b) Microscope image of the metasurfaces sample (The unit cell is marked with dotted line with the periodicity).

The generations of the metamaterials pave a new path to realize the TD resonance, which could offer opportunities for investigating the mechanism of TD resonance deeply. Since metamaterials possess unusual properties not found in nature, they have drawn considerable attention, which can be achieved by artificially arranging subwavelength unit cells at will. Thus, novel TD electromagnetic devices can be developed using metamaterials [12–15]. Both planar (2D) and 3D unit cell structures can be designed to excite TD resonance metamaterials [16–21]. 2D metamaterials (metasurfaces) are easy to be fabricated to form the functional devices.

TD resonance can be enhanced and detected by optimizing the unit cell structure of TD metamaterials. The structure of symmetric semicircle with a bar in the middle has been first demonstrated to generate TD phenomenon at microwave frequencies [22,23]. Then the similar structure was discussed expanded to terahertz frequencies, however the TD metamaterials is investigated via simulation [24]. TD resonance device was last developed at terahertz frequencies, which has exhibited rich physical phenomena and broad application prospects. TD resonances at terahertz frequencies have many applications due to their unique advantages, such as large modulation-depth modulators, high-precise biosensors, modulators, and so on, which will enrich the terahertz functional device family [25–32].

There have been numerous THz TD metamaterials proposed/fabricated with varying structures and substrates in previous research. Weak radiation has also enabled TD resonances to dominate as a promising way to achieve high Q-factors [29,30]. High-Q TD metasurfaces can be applied to highly sensitive terahertz functional devices [31]. For instance, the high Q-factors TD metasurfaces are used in high-sensitivity immune sensors, in order to measure the concentration of the SARS-CoV-2 spike protein in cells [32]. The comparison of previous researches on terahertz toroidal dipole metamaterials can be found in Table 1. The Q-factor resonances of metal-patterned metamaterials are typically low due to ohmic losses [33,34]. High Q-factor resonance was mainly realized via high Q-factor Fano structure, bound state in continuum (BIC) and quasi-bound states in the continuum (QBIC) [35–45]. As a result of the low loss of dielectric materials, the Q-factor of dielectric metamaterials were relatively high, even higher than 1000 [40]. Ruddlesden-Popper 2D perovskites were used to construct toroidal dipole metamaterials based on BIC [43]. TD dielectric metamaterials designed based on QBICs can reach high Q factor, and the Q value was high as 4990 at ~200 THz [44–46]. Active terahertz TD metamaterials can tune the electromagnetic properties of metamaterials without changing the structure of metamaterials [47,48]. Graphene was often added to the TD metamaterials in order to get the active TD metamaterial [49].

The toroidal dipole metamaterials are also designed on the solid or flexible substrate. According to Gupta et al., mirrored asymmetric split-ring resonances were fabricated on silicon substrate, which introduced to cause high Q-factor (~22) TD resonance at terahertz frequencies [50]. Then the flexible toroidal dipole is designed and fabricated on the flexible substrate, and the most used flexible substrate is polyimide. The metasurfaces's flexibility enables it to be conformal integrated onto curved or irregular objects, allowing compact, lightweight and mechanically robust devices to be developed. However, the flexible substrate metamaterials with

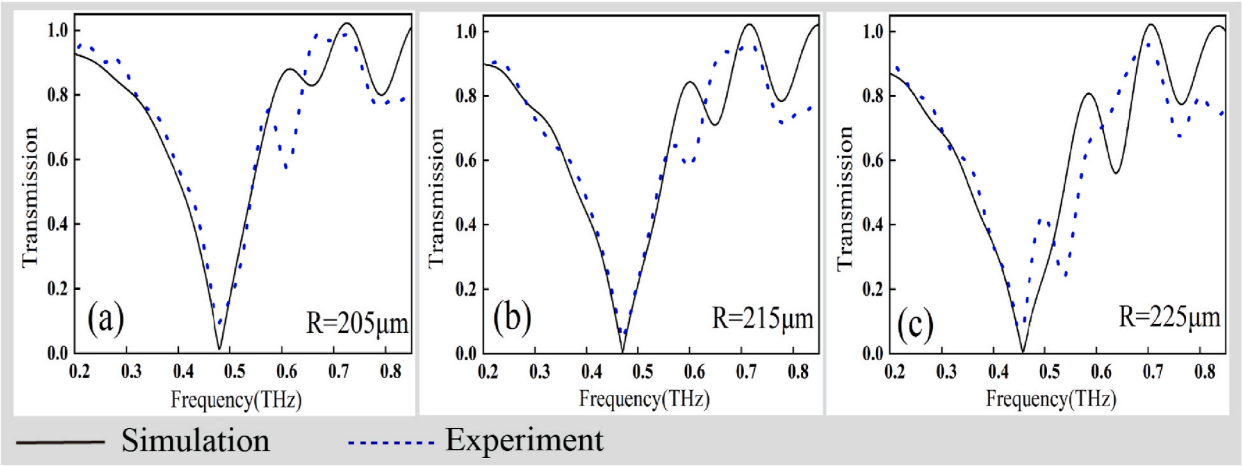

Fig. 2. Measured and simulated amplitude transmission spectra of the TD metasurfaces with various R (a) R = 205 μm (b) R = 215 μm (c) R = 225 μm.

complicated structure is still remain in the design step [51]. Only the flexible substrate metamaterials with simple structure is fabricated [20,52]. The high Q factor of flexible TD metamaterials is still in the simulation, and the Q factor of fabricated sample is often lower than the simulated one. The Q factor of flexible TD metamaterials sample is commonly lower than 20, thus the application of highly sensitive detection is limited [53,54].

This paper proposes and fabricates flexible TD metamaterials with high Q factors, which are composed of a metallic pattern layers and polyimide layers, and the metallic layer is composed of symmetric semicircle with a bar in the middle. District TD is characterized by head-to-tail arrangement of magnetic dipoles. This head-to-tail magnetic field distribution is caused by both TD resonances and current flowing through the metallic bar, and this phenomenon is discussed in detail using the power of the multipoles calculated from volume current density distributions. We propose TD metasurfaces that are easy to fabricate and have stable resonance outputs, and it offers potential applications in the THz range and allows us to realize TD's unique characteristics. Additionally, it is necessary to develop TD resonance on flexible and freestanding substrates, which can be used in a variety of applications.

2. Fabrication and simulation

Fig. 1 (a) shows a schematic diagram of TD metasurfaces with high Q-factors. Two layers are proposed on the metasurfaces: a polyimide substrate layer (20 μm thick) and a metallic pattern layer. The metallic pattern layer consists of two symmetric semicircles (outer radius R is 205 mm, inner radius SR is 189 mm) with a metal bar centered between the semicircles (the width of metal bar W is 20 μm). There is a 10 μm gap (named gap1) between the two metal bars, and a 37 μm gap (named gap2) between the two semicircles. Due to its transparency in THz and visible regimes, polyimide film was chosen as the substrate. Metasurfaces consist of periodic units, and the periodicity of the unit cell structure a × a is 480μm × 480 μm. Simulated and experimental metasurfaces samples were arranged in the x-y plane, and terahertz waves were incident along the z-axis, electric fields along the x-axis, and magnetic fields along the y-axis.

By interacting with each other, metal patterns generate TD resonances. In order to investigate the generation of TD resonances in high Q-factor TD metasurfaces, the parameter R was varied across 205, 215 and 225 μm. A variation of the W parameter also affects the electromagnetic characteristics of high Q-factor TD metasurfaces, and the variation of W (W = 30, 40, and 50 μm) parameters was also investigated.

Using conventional microelectronic preparation techniques, the proposed metasurfaces were fabricated. In the first step, a silicon wafer was spin-coated with liquid polyimide (PI-5878G HD Micro Systems TM). The thickness of the polyimide was precisely controlled by adjusting the spin rate curing and the temperature. In the second step, the metal pattern layer was fabricated using ultraviolet lithography, followed by vacuum coating with 200 nm aluminium, and finally, the samples were rinsed in acetone. In the last step, TD metasurfaces with high Q-factors were then peeled off silicon substrates. In Fig. 1(b), you can see the microscope images of the sample with R = 205 m. With THz-time domain spectroscopy (TDS), four parabolic mirrors in an 8-F confocal geometry were used to measure the electromagnetic properties of the high Q-factor TD metasurfaces [55,56]. Through the use of a parabolic mirror and bare polyimide reference, the possible dispersion was effectively reduced. Metasurfaces were attached directly to well-defined apertures at room temperature in a dry air environment (humidity<5 %). Dry air environments can effectively eliminate water vapor's ability to absorb terahertz waves.

With the commercially available software CST Microwave Studio, electromagnetic characteristics of TD were numerically simulated. Using an automatic hexahedral mesh, metasurfaces are numerically represented by their metamolecules placed in square unit cells with periodic boundary conditions along the x- and y-axes. Drude's model was used here to describe alumina metal, where angular frequency dependent permittivity is defined as $\varepsilon(\omega) = \varepsilon_\infty - \left[\omega_p^2/\omega(\omega + i\Gamma)\right]$, with damping rate of Al is 124.34×10^{12} rads^{-1}

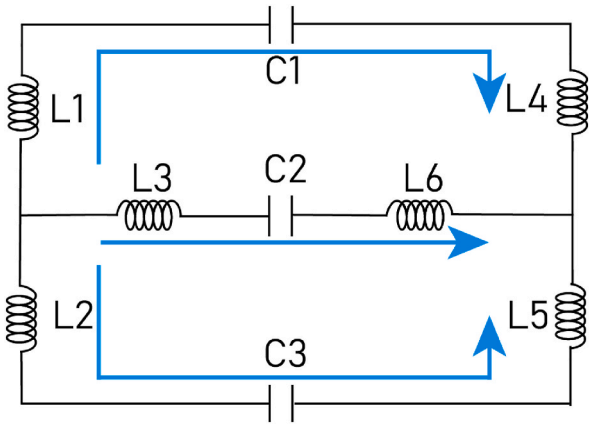

Fig. 3. LC resonant circuit.

Table 2
Theoretically calculated capacitance and inductance with different R at LFR.

R (μm)	205	215	225
C(F)	8.45e-18	1.17e-17	1.50e-17
L(H)	2.33e-29	1.50e-29	1.14e-29

and the plasma frequency of Al is 22.43 × 10^{15} rads^{-1} [57], and the dielectric constant of the polyimide ε = 3.1 × (1 +0.02i) [58].

3. Discussion

The simulated and measured transmission spectra of TD metasurfaces at R = 205 μm, 215 μm, and 225 μm are shown in Fig. 2(a), (b), and (c), where the simulated amplitude transmission spectra marked with the black solid line and the experimental amplitude transmission spectra marked with the black dashed line. Simulated and measured results are well correlated, and there are three resonances clearly visible. Interference factors such as fabrication error and measurement error may cause some deviations between simulated and measured results. Compared simulated transmission spectra with the measured results, three resonances were exhibited at ~0.47 THz, ~0.65 THz and ~0.78 THz, respectively. For the sake of simplicity, resonant dips at low frequencies will be referred to as LFRs, medium frequency dips as MFRs, and high frequency dips as HFRs. Then the inner mechanisms of the generation of TD resonance will be discussed later according to the analysis of three resonances. Fig. 2 illustrates the LFR produces a slight red shift with an increasing parameter R. This tendency was seen in the entire measured transmission spectrum, and the measured transmission spectrum showed a frequency shift of 0.02 THz in the LFR. Through inductive and capacitive couplings, the resonance of LFR can be explained by the LC resonance well.

In order to provide a more thorough explanation of the LFR, we obtain the LC equivalent circuit model of the TD metasurfaces, as shown in Fig. 3. According to Fig. 3, L1 = L2 = L4 = L5, L3 = L6, and C1=C3, where Li denoted the inductance of metal pattern and Ci denoted the capacitance of metal pattern. The capacitance and inductance at LFR can be obtained from the following equations [59]:

$$C = \frac{\varepsilon \cdot t \cdot (R - SR)}{2\pi \cdot K \cdot \mathrm{gap2}} + \frac{\varepsilon \cdot W \cdot t}{4\pi \cdot K \cdot gap1} \tag{1}$$

$$L1 = \frac{169\pi \cdot \mu_0 h \cdot R}{720(R - SR)} \tag{2}$$

$$L3 = \frac{\mu_0 h.SR}{2W} \tag{3}$$

$$L = \frac{4L1^2 \cdot L3}{2L1 + L3} \tag{4}$$

In this case, K is the constant of electrostatic force, $\mathcal{E}$ is the dielectric constant of the medium in the open gap, t is the thickness of the metallic structure, μ_0 is the vacuum magnetic permeability, and h is the thickness of the substrate on the metasurfaces.

As shown in Table 2, the capacitance and inductance with different structural parameters R are calculated by Eqs. (1)–(4). We can clearly see that the variation of C is much larger than L as R increases, then the frequencies of LFR is decreased according to $f_m = \frac{1}{2\pi\sqrt{LC}}$ (5), and the reason for the red-shift phenomenon at the LFR is clearly explained.

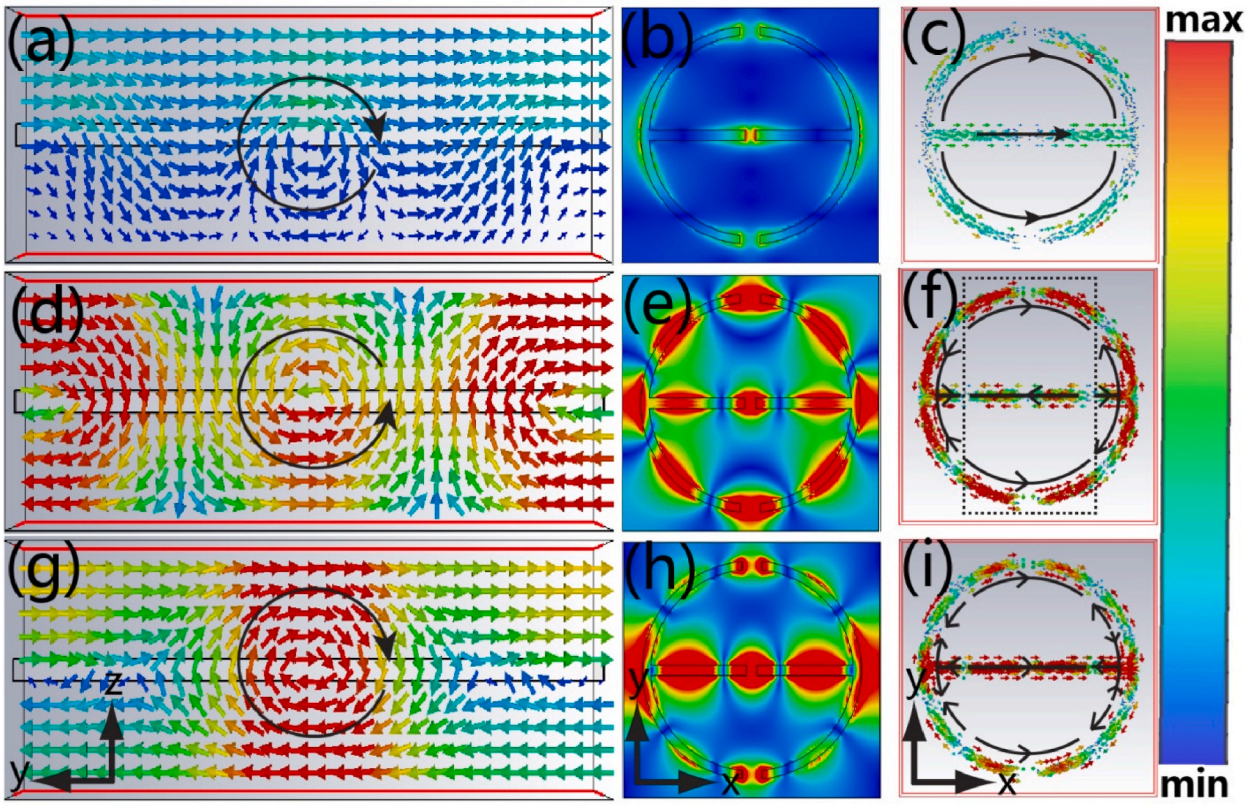

Fig. 4. Distribution of magnetic field (a) at LFR (d) at MFR (g) at HFR of the TD metasurfaces (R = 205 μm); Distribution of electric field (b) at LFR (e) at MFR (h) at HFR of the TD metasurfaces (R = 205 μm); Distribution of surface current (c) at LFR (f) at MFR (i) at HFR of the TD metasurfaces (R = 205 μm).

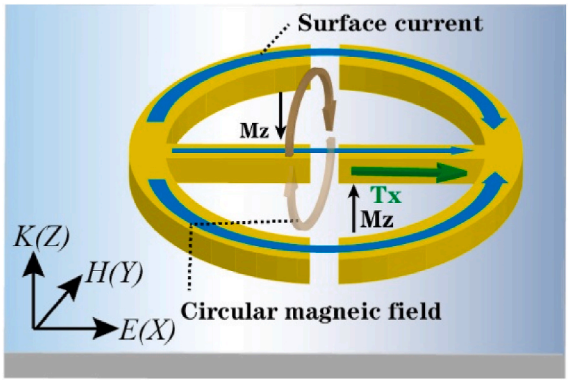

Fig. 5. Schematic of TD induced surface current by LC resonance of TD metasurfaces at LFR (the surface current indicated with blue line; Tx indicated with the green line).

Fig. 4 illustrates the magnetic field, electric field, and surface current distributions of the metasurfaces (R = 205 μm). As illustrated in Fig. 4(a)–(d) and (g), in the YZ plane at X = 0, the magnetic field distributions of LFR, MFR, and HFR are arranged head-to-tail in an annular region, and the phenomenon's generation theory was discussed in detail later.

Fig. 5 shows a schematic diagram that explains how metasurfaces generate TD resonances at LFR well. At LFR, the induced surface current formed a loop along the upper and lower semicircles with incident electric field polarization, and inductive-capacitive resonances (LCs) were formed oscillating in nature. According to the black arrows, the induced surface current flow clockwise in the upper semicircle, and the magnetic field pointing downwards; while the induced surface current flow anti-clockwise in the lower semicircle, and the magnetic field pointing upwards. As indicated by the brown circle, the magnetic vortex had a head-to-tail configuration, which is typical of TD resonances [28,29]. Meanwhile, the current flows in the middle bar also generate the magnetic loop around the bar

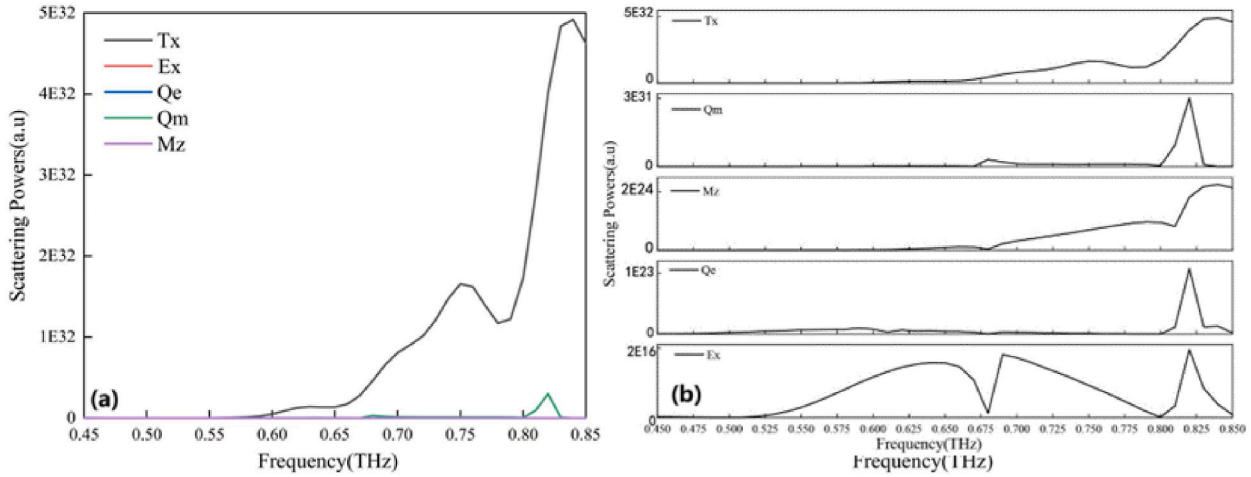

Fig. 6. (a) Decomposed scattering powers of different multipole moments in TD metasurfaces (R = 205 μm). (b) Detailed figure of decomposed scattering powers of different multipole moments in TD metasurfaces (R = 205 μm).

according to the right-hand rule. The magnetic field produced by the central bar shows a opposite to that generated by the upper and lower semicircles. Hence, the magnetic field strength is weaker than other resonances, in Fig. 4(a).

As shown in Fig. 4(e), tripoles are generated at the upper and lower semicircles, and the distribution of electric field at MFR is stronger than that of the LFR (Fig. 4 (b)). According to Fig. 4(f), we focus on the dotted square region, and the direction of magnetic field generated by the two semicircles has the same direction as the magnetic field generated by the current flowing the middle bar. The magnetic field distribution is strengthened obviously in Fig. 4(d).

Fig. 4(g) shows the strongest head-to-tail magnetic field. As shown in Fig. 4(i), the surface currents flowing the semicircle are weaker, and the middle bar's surface current is enhanced. The strength of surface current coincides with the strength of electric field in Fig. 4(h). In the middle bar, the strongest current leads to the strongest head-to-tail magnetic field distribution.

For better understanding the TD resonance in Fig. 6, we calculated the power of the five strongest multipoles based on the volume current density distribution extracted from the simulations. Using the multipole scattering theory, we quantified their contributions [30]. Toroidal dipole Tx and electric quadrupole Qe were also generated at normal incidence at THz with the electric dipole Ex parallel to the x-axis and magnetic dipole Mz parallel to the z-axis. Here are the equations to calculate Ex, Mz, Tx, Qe, Qm [60,61]:

$$\text{Electric dipole}: \mathrm{Ex} = \frac{1}{\omega}\int \mathrm{j}\,\mathrm{d}^3\mathrm{r} \tag{6}$$

$$\text{Magnetic dipole}: \mathrm{Mz} = \frac{1}{2\mathrm{c}}\int (\mathrm{r}\times\mathrm{j})\,\mathrm{d}^3\mathrm{r} \tag{7}$$

$$\text{Toroidal dipole}: \mathrm{Tx} = \frac{1}{10\mathrm{c}}\int \left[(\mathrm{r}\cdot\mathrm{j})\mathrm{r} - 2\mathrm{r}^2\mathrm{j}\right]\mathrm{d}^3\mathrm{r} \tag{8}$$

$$\text{Electric quadrupole}: \mathrm{Qe} = \frac{1}{\mathrm{i}2\omega}\int \left[\mathrm{r}_\alpha \mathrm{j}_\beta + \mathrm{r}_\beta \mathrm{j}_\alpha - \frac{2}{3}(\mathrm{r}\cdot\mathrm{j})\delta_{\alpha\beta}\right]\mathrm{d}^3\mathrm{r} \tag{9}$$

$$\text{Magnetic quadrupole}: \mathrm{Qm} = \frac{1}{3\mathrm{c}}\int \left[(\mathrm{r}\times\mathrm{j})_\alpha \mathrm{r}_\beta + (\mathrm{r}\times\mathrm{j})_\beta \mathrm{r}_\alpha\right]\mathrm{d}^3\mathrm{r} \tag{10}$$

In this equation, r is the coordinate vector with the origin in the center of the torus, c is the speed of light, and j is the density of the current. MATLAB programs were used to calculate the strength of multipoles based on simulations of current density (j).

Tx dominated the measured spectroscopy, and its density was stronger than any other multipole, as shown in Fig. 6(a). The density of Tx is almost 7 times as stronger as Mz, and Tx as has the same tendency as Mz. When we focus on HFR, the density of Tx decreased a little bit. Fig. 6(b) shows a detailed figure of a multipole to illustrate its tendency clearly. According to Fig. 4(i), a decrease in Tx coincides with the weakening of the surface current flowing in the semicircles. The surface current flowing through the middle metal bar increases, also resulting in a stronger magnetic field. In Fig. 4(g), the stronger head-to-tail magnetic field is shown, and the strongest resonance among the three resonances is attributed to the current flowing the middle metal bar. At the higher frequencies>0.8 THz), Qm, Mz, Qe values are increased dramatically, the mutual effect is much more complicated, so the variation in Fig. 6(b) is not coincide with Fig. 2.

Fig. 7(a) and (b) shows the variation of simulated and experimental Q factor, respectively. The Q factor was defined as the ratio of resonance frequency to the full width at half maximum. Fig. 7(a) and (b) shown the same tendency, when resonant frequencies

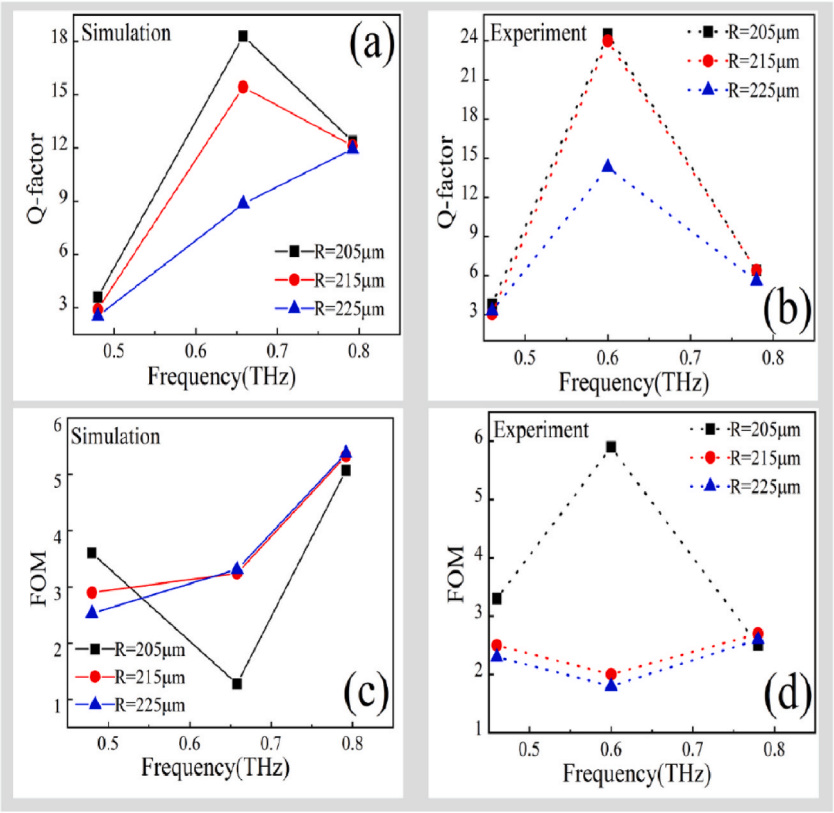

Fig. 7. (a) The variation of simulated Q factor with different R (=205 μm, 215 μm, 225 μm) at LFR, MFR and HFR. (b) The variation of experimental Q factor with different R (=205 μm, 215 μm, 225 μm) at LFR, MFR and HFR. (c) The variation of simulated FOM with different R (=205 μm, 215 μm, 225 μm) at LFR, MFR and HFR. (d) The variation of experimental FOM with different R (=205 μm, 215 μm, 225 μm) at LFR, MFR and HFR.

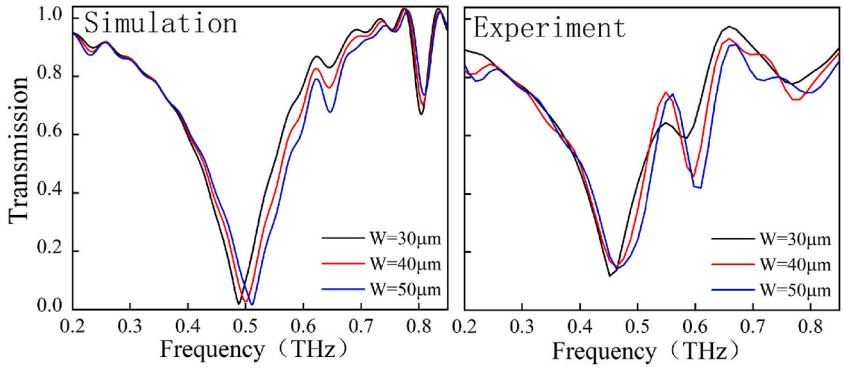

Fig. 8. Measured and simulated amplitude transmission spectra for the TD metasurfaces with various W (a) W = 30 μm (b) W = 40 μm (c) W = 50 μm.

increase, the Q value shows a trend of rising first and then falling. In Fig. 4(a) and (d), at R = 205 μm, with the increase of the resonance frequency, the head-to-tail magnetic field strength becomes stronger, and the coupling strength of the TD is increased, then the Q factor increased as a result. Q-factors can be increased by enhancing the TD response [62]. The Q factor of experimental sample is as high as 24.5, when R = 205 μm at MFR. When the frequencies are increased up to ~0.8 THz, the Q-factors is decreased, due to the complexity mutual function at higher frequencies. FOM was investigated in order to further describe the relationship between resonance intensity and the Q factor. According to equation FOM = Q*δI (11), where δI represents the resonance intensity [63]. Fig. 7(c) and (d) shows the variation of simulated and experimental FOM factor, respectively. The experimental TD metasurfaces with R = 205 μm at MFR has the highest FOM value, is expected to be applied in high-sensitivity resonant sensors [64]. The tendency of Fig. 7(c) and (d) is not the same, due to the accuracy of measured data is much lower than the simulated data.

Fig. 8 show amplitude transmission spectra simulated and measured for samples with varying values of W. As shown in Fig. 8, simulated intensity curves matched experimental results closely, with a small deviation due to a slight variation in polyimide thickness during fabrication. The frequencies of three resonances were all blue shifted as the W is increased. The head-to-tail magnetic field distributions are observed at three resonances. By tuning the parameters of W, electromagnetic characteristics can be tuned.

4. Conclusion

Metasurfaces with TDs are characterized by head-to-tail magnetic dipoles. In this research, we design and prepare the high Q-factor TD metasurfaces with a metallic pattern layer and polyimide substrate layer, the metallic pattern is consisted of aluminium symmetric semicircles with a bar in the middle. We observe three obvious resonances at LFR, MFR and HFR and three resonances show a red shift with increasing R. TD resonances at LFR produce the typical head-to-tail magnetic field distribution due to symmetric semicircles. According to Fig. 4(i), the head-to-tail magnetic field distribution becomes more pronounced as frequency increases, which is due to the flow of current in the middle metal bar. The W also can tune the electromagnetic properties in TD metasurfaces. High-Q-factor metasurfaces can be used as functional components in high-sensitivity terahertz devices.

Data availability statement

The data used to support the results of this study are included in the article. The data that support the findings of this study are openly available from [Mendeley Data] at [(https://data.mendeley.com/preview/zv4tkycwy5?a=24eec7c0-7474-4aa7-bac3-9cdcdf1a6b14].

CRediT authorship contribution statement

Shuang Wang: Writing – review & editing, Writing – original draft, Methodology, Investigation, Conceptualization. **Hai Huang:** Formal analysis, Data curation. **Quan Li:** Funding acquisition. **Chen Wang:** Resources. **Han Lei:** Writing – review & editing.

Declaration of competing interest

The authors declare that they have no known competing financial interests or personal relationships that could have appeared to influence the work reported in this paper.

Acknowledgments

This research was supported by the National Natural Science Foundation of China (62275195), and Tianjin Higher Education Technology Development Fund Project (China) (2020KJ125).

References

[1] I. Zel' Dovich, The relation between decay asymmetry and dipole moment of fundamental particles, Sov. Phys. - JETP 6 (1958) 1148–1155. https://api.semanticscholar.org/CorpusID:12856705.
[2] A. Ahmadivand, B. Gerislioglu, R. Ahujaand, Y. Mishra, Toroidal metaphotonics and metadevices, Laser Photon. Rev. 14 (11) (2020) 1900326, https://doi.org/10.1002/lpor.201900326.
[3] F. He, B. Han, X. Li, T. Lang, X. Jing, Z. Hong, Analogue of electromagnetically induced transparency with high-Q factor in metal-dielectric metamaterials based on bright-bright mode coupling, Opt Express 27 (26) (2019) 37590–37600, https://doi.org/10.1364/OE.27.037590.
[4] Y. Wang, Z. Han, Yo Du, J. Qin, Ultrasensitive terahertz sensing with high-Q toroidal dipole resonance governed by bound states in the continuum in all-dielectric metasurface, Nanophotonics 10 (4) (2021) 1295–1307, https://doi.org/10.1515/nanoph-2020-0582.
[5] X. Chen, W. Fan, Ultrahigh-Q toroidal dipole resonance in all-dielectric metamaterials for terahertz sensing, Opt Lett. 44 (23) (2019) 5876–5879, https://doi.org/10.1364/OL.44.005876.
[6] Z. Song, Y. Deng, Y. Zhou, Z. Liu, Tunable toroidal dipolar resonance for terahertz wave enabled by a vanadium dioxide metamaterial, IEEE Photon. J. 11 (2) (2019) 4600705, https://doi.org/10.1109/JPHOT.2019.2907617.
[7] T. hen, T. Xiang, J. Wang, T. Lei, F. Lu, Double E-shaped toroidal metasurface with high Q-factor Fano resonance and electromagnetically induced Transparency, AIP Adv. 11 (9) (2021) 095011, https://doi.org/10.1063/5.0057480.
[8] X. Liu, Z. Liu, M. Hua, L. Wang, K. Wang, W. Zhang, Y. Ning, Y. Shi, X. Wang, F. Yang, Tunable terahertz metamaterials based on anapole excitation with graphene for reconfigurable sensors, ACS Appl. Nano Mater. 3 (3) (2020) 2129–2133, https://doi.org/10.1021/acsanm.0c00141.
[9] X. Chen, W. Fan, H. Yan, Toroidal dipole bound states in the continuum metasurfaces for terahertz nanofilm sensing, Opt Express 28 (11) (2020) 17102–17112, https://doi.org/10.1364/OE.394416, 28.
[10] J. Xu, G. Liao, M. Gupta, M. Zhu, L. Zhuang, R. Singh, L. Chen, Terahertz microfluidic sensing with dual-torus toroidal metasurfaces, Adv. Opt. Mater. 9 (15) (2021) 2100024. https://doi/10.1002/adom.202100024.
[11] M. Lyu, Y. Shen, L. Chen, M. Zhu, L. Zhuang, Frequency selective fingerprint sensor: the Terahertz unity platform for broadband chiral enantiomers multiplexed signals and narrowband molecular AIT enhancement, PhotoniX 4 (28) (2023) 00108, https://doi.org/10.1186/s43074-023-00108-1.
[12] H. Pan, H. Zhang, Thermally tunable polarization-insensitive ultra-broadband terahertz metamaterial absorber based on the coupled toroidal dipole modes, Opt Express 29 (12) (2021) 18081–18094, https://doi.org/10.1364/OE.427554.
[13] Y. Yu, H. Zhu, B. Sun, W. Yang, Tunable Toroidal Fano Resonance in the Multiple Split-Ring Resonators Metamaterials, 2020 164936, https://doi.org/10.1016/j.ijleo.2020.164936. Optik216.
[14] M. Lyu, H. Huang, L. Chen, M. Zhu, L. Zhuang, Review on the terahertz metasensor: from featureless refractive index sensing to molecular identification, Photon. Res. 12 (2) (2024) 194–217, https://doi.org/10.1364/PRJ.508136.
[15] N. Papasimakis, V.A. Fedotov, V. Savinov, T.A. Raybould, N.I. Zheludev, Electromagnetic toroidal excitations in matter and free space, Nature Material 15 (3) (2016) 263–271, https://doi.org/10.1038/NMAT4563.

[16] E. Takou, A. Tasolamprou, O. Tsilipakos, E. Economou, Dynamic anapole in metasurfaces made of sculptured cylinders, Phys. Rev. B 100 (2019) 085431, https://doi.org/10.1103/PhysRevB.100.085431.
[17] D. Yan, M. Meng, J. Li, X. Li, Graphene-Assisted narrow bandwidth dual-band tunable terahertz metamaterial absorber, Frontiers in Physics 8 (2020) 306, https://doi.org/10.3389/fphy.2020.00306.
[18] T. Kaelberer, V. Fedotov, N. Papasimakis, D. Tsai, N. Zheludev, Toroidal dipolar response in a metamaterial, Science 330 (6010) (2010) 1510–1512, https://doi.org/10.1126/science.1197172.
[19] D. Gao, J. Zhu, R. Junsuk, L. Qi, C. Lu, B. Yin, X. Zhang, Optical toroidal dipolar response by an asymmetric double-bar metamaterial, Appl. Phys. Lett. 101 (14) (2012) 144105, https://doi.org/10.1063/1.4757613.
[20] F. Ding, K. Jiang, L. Sun, L. Wu, D. Xu, Z. Zhang, J. Yao, Stable terahertz toroidal dipolar resonance in a planar metamaterial, Phys. Status Solidi B 252 (6) (2015) 1388–1393, https://doi.org/10.1002/pssb.201552006.
[21] G. Manoj, S. Vassili, N. Xu, Q. Cong, D. Govind, S. Wang, L. Zhang, Z. Nikolay, S. Ranjan, Sharp toroidal resonances in planar terahertz metasurfaces, Adv. Mater. 28 (37) (2016) 8206–8211, https://doi.org/10.1002/adma.201601611.
[22] Alexey A. Basharin, Vitaly Chuguevsky, Nikita Volsky, Maria Kafesaki, Eleftherios N. Economou, Extremely high Q-factor metamaterials due to anapole excitation, Phys. Rev. B 95 (2017) 035104, https://doi.org/10.1103/PhysRevB.95.035104, 035104.
[23] Odysseas Tsilipakos, Zacharias Viskadourakis, Anna C. Tasolamprou, Dimitrios C. Zografopoulos, Maria Kafesaki, George Kenanakis, Eleftherios N. Economou, Meta-atoms with toroidal topology for strongly resonant responses, Micromachines 14 (2) (2023) 468, https://doi.org/10.3390/mi14020468.
[24] M.V. Cojocari, K.I. Schegoleva, A.A. Basharin, Blueshift and phase tunability in planar THz metamaterials: the role of losses and toroidal dipole contribution, Opt. Lett. 42 (9) (2017) 1700–1703, https://doi.org/10.1364/OL.42.001700.
[25] A. Ahmadiv, B. Gerislioglu, T. Noe, K. Mishra, Gated graphene enabled tunable Charge−Current configurations in hybrid plasmonic metamaterials, ACS Appl. Electron. Mater. 1 (5) (2019) 637–641, https://doi.org/10.1021/acsaelm.9b00035.
[26] X. Luo, J. Li, T. Lang, F. Jing, Z. Hong, Excitation of high Q toroidal dipole resonance in an all-dielectric metasurface, Opt. Mater. Express 10 (2) (2020) 358–368, https://doi.org/10.1364/OME.383437.
[27] J. He, L. Tian, Y. Wang, X. Jiang, X. Geng, Active modulation and switching of toroidal resonance in micromachined reconfigurable terahertz metamaterials, Results Phys. 17 (2020) 103133, https://doi.org/10.1016/j.rinp.2020.103133.
[28] B. Sun, G. Liao, J. Xu, P. Wu, L. Chen, Active switching of toroidal resonances by using a Dirac semimetal for terahertz communication, Frontiers in Physics 8 (2020) 602772, https://doi.org/10.3389/fphy.2020.602772.
[29] D. Deepak, S. Pranav, B. Sabyasachi, K. Ranjan, C. Dibakar, Multifold coupling enabled high quality factor toroidal resonances in metasurfaces, J. Appl. Phys. 127 (19) (2020) 193103, https://doi.org/10.1063/5.0007997.
[30] C. Fan, L. Zhang, H. Shen, H. Fu, Y. Wei, Q. Li, M. Soukoulis, Achieving a high- Q response in metamaterials by manipulating the toroidal excitations, Phys. Rev. 97 (3) (2018) 033816, https://doi.org/10.1103/PhysRevA.97.033816.
[31] X. Chen, K. Kaj, W. Huang, G. Zhao, D. Averitt, X. Zhang, Tunable toroidal response in a reconfigurable terahertz metamaterial, Adv. Opt. Mater. 9 (22) (2021) 2101215, https://doi.org/10.1002/adom.202101215.
[32] C. Luo, C. Wei, Y. Fan, L. Chen, R. Singh, M. Zhu, L. Zhuang, Terahertz lattice enhanced quasi-anapole immunosensor assisted by protein antibody and AuNPs, Sensor. Actuator. B Chem. 410 (1) (2024) 135628, https://doi.org/10.1016/j.snb.2024.135628.
[33] V. Stenishchev, B. Alexey, Toroidal response in all-dielectric metamaterials based on water, Sci. Rep. 7 (2017) 9468, https://doi.org/10.1038/s41598-017-07399-y.
[34] J. Khurgin, How to deal with the loss in plasmonics and metamaterials, Nat. Nanotechnol. 10 (2015) 2–6, https://doi.org/10.1038/nnano.2014.310.
[35] K. Koshelev, S. Lepeshov, M. Liu, A. Bogdanov, Y. Kivshar, Asymmetric metasurfaces with high-Q resonances governed by bound states in the continuum, Phys. Rev. Lett. 121 (2018) 193903, https://doi.org/10.1103/PhysRevLett.121.193903.
[36] W. Hsu, B. Zhen, D. Stone, D. Joannopoulos, M. Soljačić, Bound states in the continuum, Nat. Rev. Mater. 1 (2016) 16048, https://doi.org/10.1038/natrevmats.2016.48.
[37] K. Liu, D. Yong, Extreme Huygens' metasurfaces based on quasi-bound states in the continuum, Nano Lett. 18 (12) (2018) 8062–8069, https://doi.org/10.1021/acs.nanolett.8b04774.
[38] S. Han, P. Pitchappa, W. Wang, K. Srivastava, V. Rybin, R. Singh, Extended bound states in the continuum with symmetry-broken terahertz dielectric metasurfaces, Advanced Optical Materals 9 (7) (2021) 20022001, https://doi.org/10.1002/adom.202002001.
[39] R. Wang, L. Xu, Y. Wang, L. Sun, A. Jiao, Y. Meng, S. Chen, C. Chang, H. Fan, Electric Fano resonance-based terahertz metasensors, Nanoscale 28 (4) (2021) 18467–18472, https://doi.org/10.1039/D1NR04477J.
[40] T. Ma, J. Li, M. Luo, High Q-factor toroidal resonances driven by bound states in the continuum in all-dielectric metamaterial at terahertz frequencies, Opt. Laser Technol. 157 (2023) 108745, https://doi.org/10.1016/j.optlastec.2022.108745.
[41] Y. He, G.T. Guo, T.H. Feng, Y. Xu, A.E. Miroshnichenko, Toroidal dipole bound states in the continuum, Phys. Rev. B 98 (16) (2018) 161112, https://doi.org/10.1103/PhysRevB.98.161112.
[42] H.Z. Zhong, L.J. Huang, S.L. Li, C.B. Zhou, S.J. You, L. Li, Y. Cheng, A.E. Miroshnichenko, Toroidal dipole bound states in the continuum in asymmetric dimer metasurfaces, Appl. Phys. Rev. 11 (3) (2024) 031404, https://doi.org/10.1063/5.0200778.
[43] B. Saadatmand, S. Shokouhi, V. Ahmadi, M. Hamidi, Design and analysis of a flexible Ruddlesden–Popper 2D perovskite metastructure based on symmetry-protected THz-bound states in the continuum, Scientifc Reports 13 (2023) 22411, https://doi.org/10.1038/s41598-023-49224-9.
[44] P.A. Jeong, M.D. Goldflam, S. Campione, J.L. Briscoe, P.P. Vabishchevich, J. Nogan, M.B. Sinclair, T.S. Luk, I. Brener, High quality factor toroidal resonances in dielectric metasurfaces, ACS Photonics 7 (7) (2020) 1699–1707, https://doi.org/10.1021/acsphotonics.0c00179.
[45] C.B. Zhou, L.J. Huang, R. Jin, L. Xu, G.H. Li, M. Rahmani, X.S. Chen, W. Lu, A.E. Miroshnichenko, Bound states in the continuum in asymmetric dielectric metasurfaces, Laser Photon. Rev. 17 (3) (2023), https://doi.org/10.1002/lpor.202200564.
[46] S.J. You, M.M. Zhou, L. Xu, D.L. Chen, M.H. Fan, J. Huang, W.B. Ma, S.Y. Luo, M. Rahmani, C.B. Zhou, A.E. Miroshnichenko, L.J. Huang, Quasi-bound states in the continuum with a stable resonance wavelength in dimer dielectric metasurfaces, Nanophotonics 12 (11) (2023) 2051–2060, https://doi.org/10.1515/nanoph-2023-0166.
[47] N. Acharyya, S. Mallick, S. Rane, M.U. Kahaly, D.R. Chowdhury, Magnetically reconfigurable toroidal metasurfaces, Advanced Optical Material 12 (13) (2024), https://doi.org/10.1002/adom.202303045.
[48] Fedor V. Kovalev, Andrey E. Miroshnichenko, Alexey A. Basharin, Hannes Toepfer, Ilya V. Shadrivov, Active Control of Bound States in the Continuum in Toroidal Metasurfaces, ADVANCED PHOTONICS RESEARCH, 2024, https://doi.org/10.1002/adpr.202400070.
[49] Xu Chen, Wenhui Fan, Study of the interaction between graphene and planar terahertz metamaterial with toroidal dipolar resonance, Opt Lett. 42 (10) (2017) 2034–2037, 10.1364/OL.42.002034.
[50] M. Gupta, R. Singh, Toroidal versus Fano resonances in high Q planar THz metamaterials, Adv. Opt. Mater. 4 (12) (2016) 2119–2125, https://doi.org/10.1002/adom.201600553.
[51] Y. Zhao, D. Gu, H. Zhao, W. Shi, Dual terahertz slow light plateaus in bilayer asymmetric metasurfaces, Opt. Mater. Express 9 (4) (2019) 1608–1619, https://doi.org/10.1364/OME.9.001608.
[52] D. Qiu, S. Sun, X. Cheng, Y. Jin, T. Qiao, W. Zhang, X. Yang, Z. Chen, R. Li, J. Li, Q. Yao, The bound state in the continuum in flexible terahertz metasurfaces enabled sensitive biosensing, Phys. Chem. Chem. Phys. 25 (33) (2023) 222319–222324, https://doi.org/10.1039/D3CP02414H.
[53] S. Wang, L. Zhao, S. Wang, Q. Li, The investigation of the electromagnetic coupling effect in terahertz toroidal metasurfaces and metamaterials, J. Mater. Res. Technol. 9 (3) (2020) 3935–3942, https://doi.org/10.1016/j.jmrt.2020.02.019.
[54] A. Bhattacharya, M. Devi, T. Nguyen, G. Kumar, Actively tunable toroidal excitations in graphene-based terahertz metamaterials, Opt Commun. 459 (2020) 124919, https://doi.org/10.1016/j.optcom.2019.124919.

[55] D. Grischkowsky, S. Keiding, Martin van Exter, Ch Fattinger, Far-infrared time-domain spectroscopy with terahertz beams of dielectrics and semiconductors, J. Opt. Soc. Am. B 7 (10) (1990) 2006–2015, https://doi.org/10.1364/JOSAB.7.002006.
[56] K. Azad, M. Dai, L. Zhang, Transmission properties of terahertz pulses through subwavelength double split-ring resonators, Opt Lett. 31 (5) (2006) 634–636, 10.1364/OL.31.000634.
[57] A. Ordal, L. Long, J. Bell, E. Bell, R. Bell, W. Alexander, C.A. Ward, Optical properties of the metals Al, Co, Cu, Au, Fe, Pb, Ni, Pd, Pt, Ag, Ti, and W in the infrared and far infrared, Appl. Opt. 22 (7) (1983) 1099–1119, https://doi.org/10.1364/AO.22.001099.
[58] M. Ree, K. Chen K, P. Kirby, N. Katzenellenbogen, D. Grischkowsky, Anisotropic properties of high-temperature polyimide thin films: dielectric and thermal-expansion behaviors, J. Appl. Phys. 72 (5) (1992) 2014–2021, https://doi.org/10.1063/1.351629.
[59] D. Schurig, J. Mock, R. Smith, Electric-field-coupled resonators for negative permittivity metamaterials, Appl. Phys. Lett. 88 (4) (2006) 041109, https://doi.org/10.1063/1.2166681.
[60] S. Han, M. Gupta, Q. Cong, Y. Kumar, S. Ranjan, Toroidal and magnetic Fano resonances in planar THz metamaterials, J. Appl. Phys. 122 (11) (2017) 113105, https://doi.org/10.1063/1.5001246.
[61] L. Ge, L. Liu, S. Dai, J. Chai, Q. Song, H. Xiang, D. Han, Unidirectional scattering induced by the toroidal dipole moment in the system of plasmonic nanoparticles, Opt Express 25 (10) (2017) 10853–10862, https://doi.org/10.1364/OE.25.010853.
[62] P. Mishra, V. Srivastava, M. Kumar, Sunny,Polarization-Sensitive high-Q four- arm structured toroidal terahertz metamaterial, J. Electron. Mater. 50 (12) (2010) 6748–6755, https://doi.org/10.1007/s11664-021-09214-x.
[63] L. Chen, N. Xu, L. Singh, J. Cui, R. Singh, M. Zhu, L. Zhang, Defect-induced Fano resonances in corrugated plasmonic metamaterials, Adv. Opt. Mater. 5 (8) (2017) 1600960, https://doi.org/10.1002/adom.201600960.
[64] M. Manjappa, K. Srivastava, Q. Cong, I. Al-Naib, R. Singh, Active photo switching of sharp Fano resonances in THz metadevices, Adv. Opt. Mater. 29 (3) (2017) 1603355, https://doi.org/10.1002/adma.201603355.